analytical chemistry

pubs.acs.org/ac Article

Detection and Imaging of Exposure-Related Metabolites and Xenobiotics in Hard Tissues by Laser Sampling and Mass Spectrometry

Marjan Dolatmoradi, Joanna Ellis, Christine Austin, Manish Arora, and Akos Vertes*

Cite This: *Anal. Chem.* 2024, 96, 7022−7029 Read Online

ACCESS | Metrics & More | Article Recommendations | Supporting Information

ABSTRACT: The utility of two novel laser-based methods, laser ablation electrospray ionization (LAESI) and laser desorption ionization (LDI) from silicon nanopost array (NAPA), is explored via local analysis and mass spectrometry imaging (MSI) of hard tissues (tooth and hair) for the detection and mapping of organic components. Complex mass spectra are recorded in local analysis mode from tooth dentin and scalp hair samples. Nicotine and its metabolites (cotinine, hydroxycotinine, norcotinine, and nicotine) are detected by LAESI-MS in the teeth of rats exposed to tobacco smoke. The intensities of the detected metabolite peaks are proportional to the degree of exposure. Incorporating ion mobility separation in the LAESI-MS analysis of scalp hair enables the detection of cotinine in smoker hair along with other common molecular species, including endogenous steroid hormones and some lipids. Single hair strands are imaged by MALDI-MSI and NAPA-LDI-MSI to explore longitudinal variations in the level of small molecules. Comparing spectra integrated from NAPA-LDI-MSI and MALDI-MSI images reveals that the two techniques provide complementary information. There were 105 and 82 sample-related peaks for MALDI and NAPA, respectively, with an overlap of only 16 peaks, indicating a high degree of complementarity. Enhanced molecular coverage and spatial resolution offered by LAESI-MS and NAPA-LDI-MSI can reveal the distributions of known and potential biomarkers in hard tissues, facilitating exposome research.

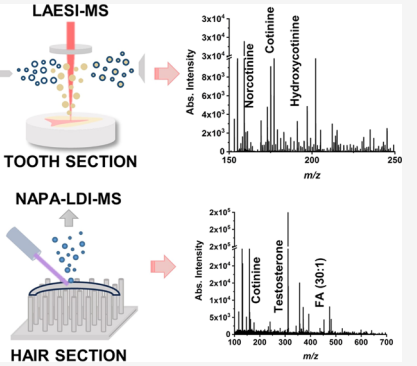

INTRODUCTION

Beyond genetic disposition, human health throughout life is greatly influenced by environmental factors. Capturing the chemical signatures of these factors in an organism can inform us of past exposures and possess the prognostic value for future health. The most widely used approaches for measuring exposure-related biomarkers rely on the analysis of biological fluids, including blood plasma and serum, and urine.[1] Sustained environmental exposure also results in altered composition of hard tissues, including teeth and hair. Studying the related chemical species in archeological and contemporaneous specimens—collectively called the exposome—can inform us of dietary habits, food sources, and human migration.[2,3] In most previous investigations, changes in trace elemental composition or stable isotope ratios have been captured by inductively coupled plasma (ICP) mass spectrometry (MS) coupled to laser ablation (LA) microsampling for localization and distribution information.[4,5] By breaking down the molecules into their atomic constituents, LA−ICP−MS reveals a wealth of information about elemental abundance variations. Determining changes in the organic components of hard tissues, including peptides, metabolites, and xenobiotics, a far less frequent undertaking, requires sampling and ionization techniques resulting in no or minimal ion fragmentation.[6,7]

As during prenatal and childhood development the dentin in teeth builds up layer by layer, the resulting growth lines can be correlated to biological age. The composition of each layer can reflect sustained environmental exposure during the related period.[8] Recent studies of organic components in deciduous teeth by liquid chromatography (LC)−MS have relied on grinding and analyzing an entire tooth, resulting in mixing the components from three different tissue types, i.e., enamel, dentin, and pulp, therefore preventing the discovery of exposure timing.[9,10] Using local analysis, dating of the exposure becomes possible, and the spatial resolution of the analysis can be translated into time resolution during development.[11−13] Recently, by selectively sampling dentin layers, the detection of phthalates, bisphenols, parabens, and nicotine metabolites has been demonstrated, and their abundances in particular dentin layers have been correlated with the time of the environmental exposure.[14] It is anticipated that higher spatial resolution, e.g.,

Received: January 11, 2024
Revised: March 22, 2024
Accepted: April 15, 2024
Published: April 26, 2024

https://doi.org/10.1021/acs.analchem.4c00224
Anal. Chem. 2024, 96, 7022−7029

on a micrometer scale, in the analysis of deciduous teeth translates into finer temporal resolution during development.

Soft ionization methods, such as electrospray ionization (ESI) and matrix-assisted laser desorption ionization (MALDI), are extensively used for the detection of metabolites, peptides and proteins, and for the determination of their distribution in soft tissues using MS imaging (MSI).[15] Sample preparation for these methods, however, can lead to a reduction in spatial resolution for metabolites and to spectral interferences. For example, for ESI the sample must be dissolved, resulting in a complete loss of spatial distribution information for the detected chemical species. In the case of MALDI, an exogenous matrix has to be deposited to absorb the laser radiation and cocrystallized with the analytes of interest in the surface of the tissue sample. Ions generated from the MALDI matrix often interfere with the sample-related ions below m/z 500, thereby interfering with the detection of ions from numerous small metabolites and xenobiotics.

Laser ablation electrospray ionization (LAESI) is an ambient ionization technique that requires no addition of an external matrix because the utilized mid-IR laser radiation (λ = 2.94 μm) efficiently ablates most tissues and cells with high water content.[16] It has been used for local MS analysis with a spatial resolution of ~50 μm, two- and three-dimensional MSI of soft animal and plant tissues, and for single-cell analysis.[17−19] Despite the benefits of minimal sample preparation required for LAESI−MS and MSI, their application for hard tissue analysis has not yet been demonstrated.

Another approach to avoid spectral interference resulting from the matrix is by implementing matrix-free laser desorption ionization (LDI) methods. Silicon nanopost arrays (NAPAs) serve as a highly efficient nanophotonic ionization platform.[20] It has been shown to detect ultratrace amounts of analytes (e.g., 800 zmol of verapamil in a standard solution), molecular imaging capabilities by MSI, and molecular coverage complementary to MALDI.[21−23] Although a limited number of MALDI−MS and MSI applications have been demonstrated for bone samples, these studies focus on collagen fingerprinting and marrow lipids.[24,25] Profiling and two-dimensional imaging of drugs of abuse (e.g., cocaine) and medications (e.g., zolpidem) in single hair strands have been demonstrated by MALDI−MS.[26,27] Drug incorporation into hair can progress through multiple mechanisms, resulting in large variations in inclusion rates.[28] Comparison of untargeted analysis of urine samples by MALDI−MS and NAPA−LDI−MS revealed that the former provided better coverage for larger compounds, whereas the latter showed superior performance for smaller molecules.[23] It is unclear to what degree the complementarity of NAPA−LDI and MALDI in molecular coverage carries over to hard tissue samples.

In this study, the utility of two novel laser-based soft ionization methods, LAESI and NAPA−LDI, is explored via the local analysis and MSI of tooth and hair samples for the detection of organic components with improved spatial resolution. In the local analysis mode, both techniques yield complex mass spectra from tooth dentin and scalp hair. Comparison of molecular imaging by NAPA−LDI−MSI and MALDI−MSI for hair reveals that they also provide complementary information for hard tissues.

METHODS

The chemicals and supplies used for MS and MSI with LAESI, NAPA−LDI, and MALDI ion sources have been described in previous publications.[16,21−23,29] Here, we emphasize the materials and experimental parameters that are specific for hard tissue analysis. In all three methods, the laser fluence is carefully adjusted to ensure optimal sampling and ionization, minimizing sample degradation and ion fragmentation. The optimal laser fluence varies depending on the laser pulse characteristics (e.g., wavelength and pulse length) and the properties of the analyzed tissue and/or the matrix (nonlinear light absorption at the laser wavelength, phase transition temperatures, and tensile strength). Compared to soft tissues, teeth, and hair require higher laser fluences for effective sampling and ionization. Owing to the wide variety of material properties for hard tissues, selecting the appropriate laser fluence requires an optimization procedure for each sample type.

LAESI−MS. Past applications of LAESI−MS have demonstrated that it requires minimal sample preparation and is well suited for the analysis of water-containing samples.[16] The experimental details of the method are covered in previous publications.[30] Briefly, mid-IR laser pulses at a 2.94 μm wavelength were produced by a Nd:YAG laser-driven optical parametric oscillator (Vibrant IR, Opotek, Carlsbad, CA) with a 4 ns pulse length at up to a 100 Hz repetition rate. They were focused to an ~150 μm spot on the sample through a 100 mm focal length CaF_2 plano-convex lens (LA5010, Thorlabs, New Jersey) (see Figure S1a). To avoid spectral interferences from the embedding medium, a long-distance video microscope equipped with a 10× objective lens (MY10X-803, Thorlabs, Newton, NJ) and a CCD camera (DCU223M-GL, Thorlabs, Newton, NJ) was utilized for precise observation and positioning of the laser focal spot. Thus, the obtained mass spectra were collected from dentin without interference from the surrounding resin. The laser ablation induced an expanding plume that was intercepted and ionized by an electrospray, positioned on the axis with the inlet orifice of the mass spectrometer. The spectra were acquired by a Synapt G2-S mass spectrometer (Waters Co., Milford, Massachusetts) equipped with traveling wave ion mobility separation (TW-IMS).[31]

Molar and incisor teeth were extracted from rat jaws using dental forceps, and any adhering soft tissue was removed by scraping with a scalpel before washing with Milli-Q water. Exfoliated human deciduous (baby) teeth were cut along the labio-lingual/labial-buccal plane using a diamond-encrusted blade on a low-speed saw (IsoMet Low Speed, Buehler, Lake Bluff, Illinois). Rat teeth and human teeth offcuts were then embedded in resin, ground, and polished to a final 1 μm finish using a diamond paste (MetaDi Ultra Paste, Poly, 1 μm, Buehler, Lake Bluff, Illinois). The epoxy embedding medium for teeth was made by combining resin and hardener (EpoxiCure, Buehler, Lake Bluff, Illinois). The diamond paste residue was washed from the resin block surface by sonication in Milli-Q water. Male rats were exposed to "low" (0.2 mg) or "high" (2 mg) levels of nicotine.

Direct analysis of rat molar and incisor tooth sections was performed by LAESI-MS in both positive and negative ion modes. In positive ion mode, the electrospray solution consisted of 50% methanol acidified with 0.1% glacial acetic acid (v/v), and in negative ion mode, 2:1 (v/v) methanol/chloroform solution was used. The spray solution was supplied by a syringe pump (Physio 22, Harvard Apparatus, Holliston, Massachusetts) at 400 nL/min through a stainless-steel emitter with a 100 μm inner diameter (MT320-100-5-5, New

https://doi.org/10.1021/acs.analchem.4c00224
Anal. Chem. 2024, 96, 7022−7029

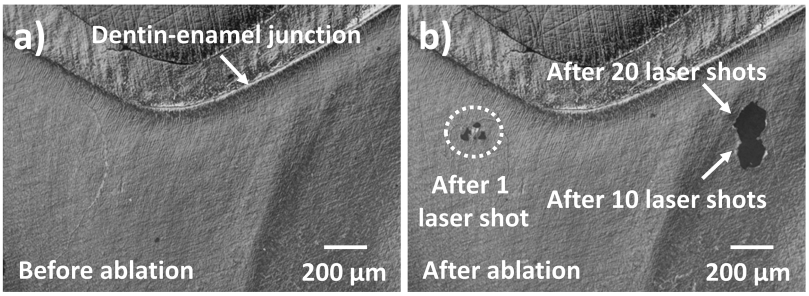

Figure 1. (a) Brightfield optical microscopic image of human tooth section before ablation. The section was cut along the labio-lingual/labial-buccal plane. (b) Ablation craters in dentin created by 1, 10, and 20 mid-IR laser pulses.

Objective, Woburn, Massachusetts). High voltages of +3500 V in positive ion mode and −2600 V in negative ion mode were provided by a regulated power supply (PS350, Stanford Research Systems, Sunnyvale, California).

To demonstrate the feasibility of direct hair analysis, scalp hair samples were collected from nonsmoker (a female taking oral contraceptive pills) and smoker (a male) volunteers. As the focus was on the presence or absence of a xenobiotic, nicotine, and its metabolites in hair in correlation to smoking, the importance of gender- and age-matched samples was not paramount. Before the analysis of hair samples, surface contamination had to be removed to avoid interference with metabolite detection. For decontamination, a 5 min wash with sodium dodecyl sulfate was followed by a 5 min wash with pure methanol.[32] For the LAESI-MS analysis of hair samples, TW-IMS was engaged to separate structural isomers and quasi-isobaric species based on their collision cross section ($^{TW}CCS_{N2}$) values. To maximize ion separation by IMS, optimum values were found for the drift gas flow rate (90 mL/min), wave velocity (650 m/s), and wave height (40 V).

Mass spectra were acquired and processed with MassLynx 4.1 software (Waters, Milford, MA). Utilizing poly-DL-alanine standards (P9003, Sigma-Aldrich) and the DriftScope software (Version 2.8, Waters Co., Milford, Massachusetts), $^{TW}CCS_{N2}$ values were extracted for selected ions and were searched against the AllCCS database (http://allccs.zhulab.cn/, last visited on January 10, 2024). During calibration, the observed maximum ΔCCS value for alanine oligomers was ±5 Å^2. Therefore, for most assignments, this ΔCCS value was used as a cutoff. As of May 2023, the AllCCS database contained >7700 experimental CCS values for >4300 compounds, and >14 300 000 predicted CCS values for >2 000 000 compounds. In this study, most measured CCS data were compared to values predicted by machine learning, especially for ionic species with water loss, for example, $[M + H - H_2O]^+$. Tandem MS was performed by collision-induced dissociation (CID), and the measured fragmentation patterns were searched against the MoNA database (https://mona.fiehnlab.ucdavis.edu/, last accessed January 10, 2024). Tentative assignments for sample-related peaks were based on accurate masses, isotope distribution patterns, tandem mass spectra, CCS values, and database searches (Human Metabolome Database, HMDB Ver. 5, https://hmdb.ca/, last visited on January 10, 2024). To optimize the limit of detection, the sensitivity mode of the mass analyzer was engaged, resulting in reduced mass accuracy in some cases. Nevertheless, mass accuracy and CCS errors at $\Delta m/z$ < 10 mDa and ΔCCS < 5 Å^2, respectively, were acceptable for this instrument.

MALDI−MS and NAPA−LDI−MS. Details for MALDI−MS and NAPA−LDI−MS local analysis and imaging are described in the recent literature.[22,23] Briefly, data acquisition for MALDI and NAPA−LDI was performed on a MALDI−LTQ−Orbitrap XL mass spectrometer (Thermo Fisher Scientific Inc., Bremen, Germany). The instrument was equipped with a nitrogen laser (Model MNL-100, LTB Lasertechnik Berlin GmbH, Germany) emitting 3 ns pulses at 337 nm with a 60 Hz repetition rate and generating a focal spot size of ∼100 μm × 80 μm. Laser fluences were 16 and 60 mJ/cm^2 for MALDI−MS and NAPA−LDI−MS, respectively, and spectra were collected with 5 laser shots/scan.

The nanofabrication process for NAPA chip production has been described previously in detail.[33] Briefly, low-resistivity p-type silicon wafers (Silicon Valley Microelectronics, Inc., Santa Clara, California) were used to fabricate NAPA imaging chips by using deep UV projection lithography (DUV-PL) followed by deep reactive ion etching (DRIE). Posts with dimensions of 1100 nm in height and 150 nm in diameter were fabricated with a periodicity of 337 nm to achieve a maximum ion yield (see Figure S1b).

Cotinine standard (74003, Sigma-Aldrich, St. Louis, Missouri) was prepared at a 1.0 mM concentration. The MALDI matrix, α-cyano-4-hydroxycinnamic acid (CHCA) (C8982, Sigma-Aldrich, St. Louis, Missouri) was dissolved at a 10 mg/mL concentration in 75:25 (v/v) acetonitrile/water acidified with 0.2% trifluoroacetic acid. For MALDI−MS, the cotinine standard and matrix solutions were mixed at a 1:2 ratio, and 1.5 μL of the resulting solution was deposited onto a stainless-steel sample plate and left to dry at atmospheric pressure. For NAPA−MS, 250 nL of the 1.0 mM cotinine standard solution was deposited onto a NAPA chip and allowed to dry before analysis.

Washed hair samples were embedded in a 2.5% carboxymethyl cellulose (CMC) solution in a mold. A block of frozen embedding medium was placed on top of the sample to produce a flat hair surface for sectioning. After the embedding medium was frozen, it was placed in a cryomicrotome operated at −15 °C, and 12 μm-thick hair sections were cut (literally splitting hair) for both MALDI−MSI and NAPA−LDI−MSI experiments. The sections were thaw-mounted onto Superfrost Plus microscope slides and NAPA imaging chips for MALDI−MS and NAPA−LDI−MS analyses, respectively (see Figure S4). For dehydration, the samples were placed in a vacuum desiccator for 30 min before analysis.

For MALDI−MSI experiments, the CHCA matrix solution was applied on top of the sample using an oscillating capillary nebulizer 15−20 times alternating between spraying for 10 s and drying for 30 s. This resulted in a total matrix solution

https://doi.org/10.1021/acs.analchem.4c00224
Anal. Chem. 2024, 96, 7022−7029

deposition of 132 μL, with a final coating density of ∼4.2 μg/mm^2. For MALDI- and NAPA−LDI−MSI, laser fluences of 80 and 119 mJ/cm^2 were used, respectively. The raster step size was set to 100 μm, allowing for sampling without significant gaps between the analyzed spots along the hair tissue section. The acquisition range was set to m/z 50−2000 for both ionization methods. A ProteoMass MALDI Calibration Kit (MSCAL4, Sigma-Aldrich, St. Louis, Missouri) was used for instrument calibration prior to analysis.

Data acquisition and analysis were performed by Xcalibur (3.0.63) software, and the imaging data were visualized by ImageQuest (1.1.0) (Thermo Fisher Scientific Inc., Bremen, Germany). Peak annotations were based on accurate mass, tandem MS, and database search (Human Metabolome Database, HMDB Ver. 5, https://hmdb.ca/, last visited on January 10, 2024).

RESULTS AND DISCUSSION

Analysis of Metabolites in Teeth and Single Hair Strands Using LAESI−MS. Although bulk and physical segmentation-based analyses of deciduous teeth are reported in the literature, to improve the spatial resolution, laser-based sampling techniques are desirable. The studied hard tissue samples included longitudinal sections of molars and incisors from rats exposed to tobacco smoke, human deciduous molars, and human scalp hair. In Figure 1a, the brightfield image of a human tooth section is shown around the dentin-enamel junction, revealing both mineralized tissues.[34] Laser fluence, pulse repetition rate, and number of delivered laser pulses were optimized to obtain well-defined craters and reliable spectra from the samples. The laser fluence was precisely set above the ablation threshold of the tissue for effective ablation and ionization of the analytes of interest. However, excessive fragmentation and degradation of materials had to be prevented. In Figure 1b, ablation craters in the dentin are shown for 1, 10, and 20 pulses delivered at a 2.2 J/cm^2 fluence and a 10 Hz repetition rate. After 10 laser shots were fired per analyzed spot, well-defined ablation craters were obtained. Displacing the analyzed spots by ≥150 μm resulted in clear separation that enabled the mapping of spatial distributions and the linear profiling of metabolites.

After optimization of the laser ablation parameters, the setup was coupled to the LAESI ion source and the mass spectrometer. In Figure 2a, a positive ion mode mass spectrum is shown from the local analysis of molar dentin from rats exposed to tobacco smoke. Tentative peak assignments are supported by close matches between measured and calculated m/z values for nicotine ($\Delta m/z$ = 2.0 mDa) and its metabolites, cotinine ($\Delta m/z$ = 0.2 mDa for $[M + H]^+$ and $\Delta m/z$ = 9.0 mDa for $[M - H_2O + H]^+$), hydroxycotinine ($\Delta m/z$ = 7.0 mDa for $[M + H]^+$ and $\Delta m/z$ = 6.0 mDa for $[M - H_2O + H]^+$), and norcotinine ($\Delta m/z$ = −3.0 mDa). Intensity ratios for these peaks in the mass spectra from the teeth of rats exposed to "high" and "low" levels (10:1) of nicotine indicated I_{high}/I_{low} = 5.4 ± 0.6 (n = 5) for nicotine incorporated into the teeth, I_{high}/I_{low} = 9.1 ± 1.2 (n = 5) for cotinine, I_{high}/I_{low} = 1.9 ± 0.6 (n = 5) for hydroxycotinine, and I_{high}/I_{low} = 3.1 ± 0.5 (n = 5) for norcotinine. Differences in the intensity ratios of hydroxycotinine and norcotinine compared to that of cotinine are a result of multiple factors, including the enzyme-mediated nicotine metabolism in the liver, the distribution of these compounds in the body, and their excretion. Cotinine, a major metabolite of nicotine, undergoes transformation through two

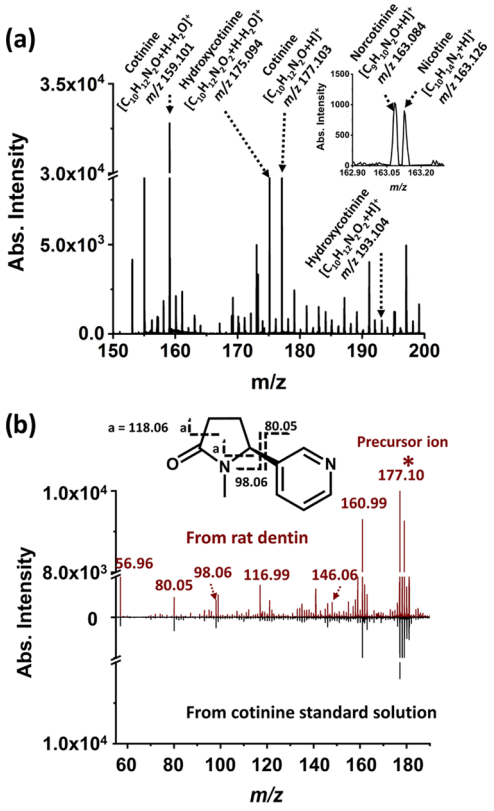

Figure 2. (a) Positive ion mode LAESI mass spectrum from local analysis of rat molar dentin exposed to tobacco smoke. Tentative peak assignments are supported by close matches between measured and calculated m/z values for nicotine ($\Delta m/z$ = 2.0 mDa) and its metabolites, cotinine ($\Delta m/z$ = 0.2 mDa for $[M + H]^+$ and $\Delta m/z$ = 9.0 mDa for $[M - H_2O + H]^+$), hydroxycotinine ($\Delta m/z$ = 7.0 mDa for $[M + H]^+$ and $\Delta m/z$ = 6.0 mDa for $[M - H_2O + H]^+$), and norcotinine ($\Delta m/z$ = −3.0 mDa). (b) Comparison of tandem mass spectra for m/z 177.103 precursor ion (*) obtained from (top) rat molar dentin and (bottom) cotinine standard solution.

processes catalyzed by the liver enzyme cytochrome P450 2A6 (CYP2A6), hydroxylation and N-demethylation, resulting in the formation of 3-hydroxycotinine and norcotinine, respectively.[35] The lower abundances of these two metabolites and the smaller intensity ratios can be associated with variation in the rate of cotinine metabolism (CYP2A6 activity) and the rate of excretion of the reaction products.

To enhance the reliability of the peak assignment for m/z 177.1029 as cotinine, tandem MS (LAESI−MS/MS) was performed using CID at a 15 eV collision energy. Figure 2b shows a comparison of the tandem mass spectra for the m/z 177.1029 precursor ions obtained from rat dentin and a 1.0 mM cotinine standard solution. The fragmentation patterns were similar in the m/z 50−180 range.

For the local analysis of single hair samples, the mid-IR laser ablation conditions had to be adjusted. The best results were observed at a 10 Hz repetition rate, 20 laser shots per analyzed spot, and a laser fluence of 3.3 J/cm^2. The micrograph of the ablation marks on a hair strand is shown in Figure 3a, and the corresponding positive ion mode LAESI mass spectrum is shown in Figure 3b. The spectra collected from the hair strand were background subtracted and de-isotoped. The accurate masses of the detected peaks, along with the fragmentation patterns from tandem MS and the measured CCS values, were used for peak assignments. As shown in Figure 3c, the cotinine

https://doi.org/10.1021/acs.analchem.4c00224
Anal. Chem. 2024, 96, 7022−7029

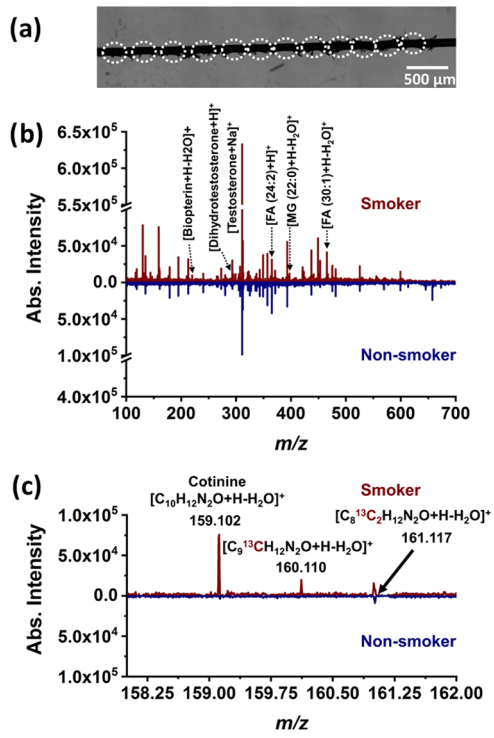

Figure 3. Positive ion mode LAESI−IMS−MS of human scalp hair collected from male smoker and female nonsmoker volunteers. (a) Ablation marks along the hair strand, produced by 20 laser shots, are indicated by dashed circles. (b) Comparison of mass spectra from hair strands of smoker and nonsmoker individuals. (c) A cotinine-related ion, $[M + H - H_2O]^+$, at m/z 159.102 and its isotope pattern were only detected for the smoker hair.

ion with water loss, $[M + H - H_2O]^+$, also observed in the analysis of teeth dentin, was detected for smoker scalp hair. The isotope distribution pattern and the measured $^{TW}CCS_{N2}$ value of 129.1 Å^2 (ΔCCS = −4.4 Å^2) also support the ion annotation. Comparison of the spectra in Figure 3c for the smoker and nonsmoker samples indicates the lack of cotinine signal for the latter.

Comparison of mass spectra for male smoker and female nonsmoker samples, obtained by averaging over three ablation marks in each hair strand, revealed 77 and 87 sample-related peaks, respectively, with a total of 50 common spectral features (Figure 3b). To identify the spectral features of significantly regulated species, a volcano plot was constructed with fold change cutoffs of FC $\geq$ 2 and FC $\leq$ 0.5, and a statistical significance cutoff of 99.5% corresponding to $p \leq 0.05$ (see Figure S2). Analysis of the LAESI−MS data demonstrated that 10 spectral features were significantly more abundant in the hair of the male smoker, whereas 24 peaks showed higher intensity in the sample from the female nonsmoker. For example, m/z 159.102, tentatively assigned as cotinine, showed a significant increase with FC = 7.4 (p = 0.002) in signal intensity for male smoker compared to the female nonsmoker sample.

The ionic species detected at m/z 291.226 (see Figure 3b) with $^{TW}CCS_{N2}$ = 171.9 Å^2 was putatively assigned to protonated dihydrotestosterone (DHT) ($\Delta m/z$ = −6.0 mDa; ΔCCS = −4.8 Å^2). It is one of the most potent androgens that regulates hair growth. DHT exhibited an FC = 0.18 (p = 0.007) for the smoker male to nonsmoker female ratio.

Absolute serum concentrations for DHT had been determined by LC−MS/MS.[36] Ranges for healthy adult men (n = 113) and healthy premenopausal women (n = 113) were 0.47−2.65 and 0.09−0.91 nmol/L, respectively. Considering that the serum levels of DHT in women taking oral contraceptives is known to double, a low male to female DHT abundance ratio in such cases can occur.[37] Additionally, differences can originate from comparing hair samples as opposed to serum. DHT is synthesized from testosterone by 5α-reductase in various tissues including hair follicles, and along with testosterone acts as a key factor in hair growth.[38]

The spectra in Figure 3b exhibit additional hormone-related peaks. For example, testosterone at m/z 311.195 ($[M + Na]^+$) with $^{TW}CCS_{N2}$ = 189.9 Å^2 ($\Delta m/z$ = −4.0 mDa; ΔCCS = −6.8 Å^2)[39] was detected in both hair samples. Tandem MS for m/z 311.195 resulted in the generation of a single fragment at m/z 293.178, consistent with the MS/MS spectrum of sodiated testosterone in the database (https://mona.fiehnlab.ucdavis.edu/spectra/display/UF416035). Previous work on the levels of steroid hormones in human hair was based on gas chromatography (GC)−MS and LC−MS techniques.[40] The ∼2 times greater testosterone ion abundances observed in male hair are consistent with the ratio of gender-specific absolute concentrations in the literature (2.7 and 1.7 ng/g in male and female hair, respectively).[41]

Future applications of LAESI−MS are envisioned for detecting longitudinal variations in steroid hormone levels in male and female hair that are of interest in the study of long-term hormonal changes. Whereas inter-day variations in hormone levels have been explored using biofluids,[42] detecting the levels of deposited hormones in hair during hair growth might provide additional insight into the patterns of endogenous steroid hormone secretion on a longer time scale.

Among the species observed in both spectra in Figure 3b, m/z 220.087 was tentatively assigned as the ion formed by water loss from the protonated biopterin ion ($\Delta m/z$ = 4.0 mDa). The difference between the measured $^{TW}CCS_{N2}$ = 150.5 Å^2 for this ion and the predicted CCS = 149.4 Å^2 in the AllCCS database, ΔCCS = 1.1 Å^2, was within the experimental uncertainty of the measurement (<5 Å^2). For further verification of the assignment, tandem MS of the m/z 220.087 ion was performed with CID at 25 eV, and fragments with m/z 203.065, 193.109, and 177.076 were detected (see Figure S3). Comparison of the fragmentation pattern ions with those of biopterin in a tandem MS database (https://mona.fiehnlab.ucdavis.edu/spectra/display/MoNA019779) confirmed the detection of this compound in the human hair sample. This metabolite was also detected in the hair follicle at a much higher intensity compared to the hair shaft (data not shown). Previous studies have demonstrated that tetrahydrobiopterin plays an important role in melanocyte survival and pigmentation, and can also affect the differentiation of keratinocytes.[43]

Trace levels of endogenous lipids are also noted in the spectra in Figure 3b. In addition to proteins that account for the bulk of human hair (65−95% is keratin), several lipid classes including free fatty acids, phytosphingosine, and ceramide are also present at levels of 1−9%.[44,45] The peaks detected at m/z 365.342 with $^{TW}CCS_{N2}$ = 201.2 Å^2, m/z 397.363 with $^{TW}CCS_{N2}$ = 214.2 Å^2, and m/z 465.422 with $^{TW}CCS_{N2}$ = 215.2 Å^2 (see Figure 3b) were assigned to protonated FA (24:2) ($\Delta m/z$ = −1.0 mDa, ΔCCS = 3.5 Å^2), protonated MG (22:0) ($\Delta m/z$ = −5.1 mDa, ΔCCS = 4.7 Å^2)

https://doi.org/10.1021/acs.analchem.4c00224
Anal. Chem. 2024, 96, 7022−7029

with water loss, and protonated FA (30:1) (with $\Delta m/z$ = −8.0 mDa and ΔCCS = −5.1 Å^2) with water loss, respectively. Identification of additional spectral features requires more work. Beyond the accurate masses and CCSs, tandem MS measurements are needed for peak assignments.

Profiling of Metabolites in Single Hair Strands. The molecular composition of human scalp hair can reflect the diet, substances ingested over time, and environmental exposure. As head hair growth rates are estimated to be ∼10 mm/month (∼330 μm/day),[27] longitudinal spatial profiling of hair composition can reveal time-dependent environmental exposure and drug ingestion. In order to capture daily compositional variations, a spatial resolution of 100 μm is sufficient.

To explore the impact of matrix interferences and expand the molecular coverage of the analysis, we tested the utility of both MALDI−MSI and the matrix-free NAPA platform for LDI−MSI. The response of the two techniques for cotinine, an analyte often targeted in tobacco smoke exposure studies, and mass spectra of standards were acquired in positive ion mode (not shown). Detection of the protonated cotinine molecule at m/z 177.100 was achieved by both platforms, but NAPA−LDI−MS resulted in a significantly cleaner spectrum (no matrix peaks). A smaller sodiated cotinine peak was also detected by NAPA−LDI−MS, as this method has a stronger tendency to form alkali metal adduct species.[23]

Spectra integrated from MALDI−MSI and NAPA−LDI−MSI images were compared for single hair samples. For the imaging, the ∼120 μm diameter hair strand of a female volunteer using hormonal contraceptives was cut into 12 μm-thick longitudinal sections and mounted on microscope slides and NAPA imaging chips (see Figure S4a,b, respectively).[23,46] For MALDI−MS, the CHCA matrix was deposited on top of the sample, whereas NAPA−LDI−MS required no additional processing. Molecular coverages of the two techniques were compared in the positive ion mass spectra (Figure 4a). Although for both MALDI−MS and NAPA−LDI−MS the signal intensity decreased at higher m/z values, the intensity drop occurred more quickly for the latter. This result was consistent with our earlier findings for urine samples.[23] To assess the complementarity of the spectral features captured by the two platforms, sample-related peak lists were extracted from the spectra integrated over the images. There were 105 and 82 sample-related peaks for MALDI and NAPA, respectively, with an overlap of only 16 peaks, indicating a high degree of complementarity.

Chemical images of the longitudinal hair sections were investigated for the two platforms (Figure 4b). Whereas ions at m/z 383.180 and m/z 369.348 were detected at high intensities by MALDI (∼3 × 10^5 and ∼5 × 10^5 counts, respectively), weak to no ion intensities were observed by LDI from NAPA. Conversely, compared to negligible signal by MALDI, significant ion intensities for m/z 313.208 (∼7 × 10^4 counts) were detected by NAPA, further demonstrating spectral complementarity.

The periodicity observed in some of the images (periods ranging from ∼100 to ∼300 μm) could be attributed to stepwise sampling by the laser. Although the rectangular sampling grid had a 100 μm periodicity, the hair strand did not line up with the pattern, resulting in larger and variable distances between the interrogated spots.

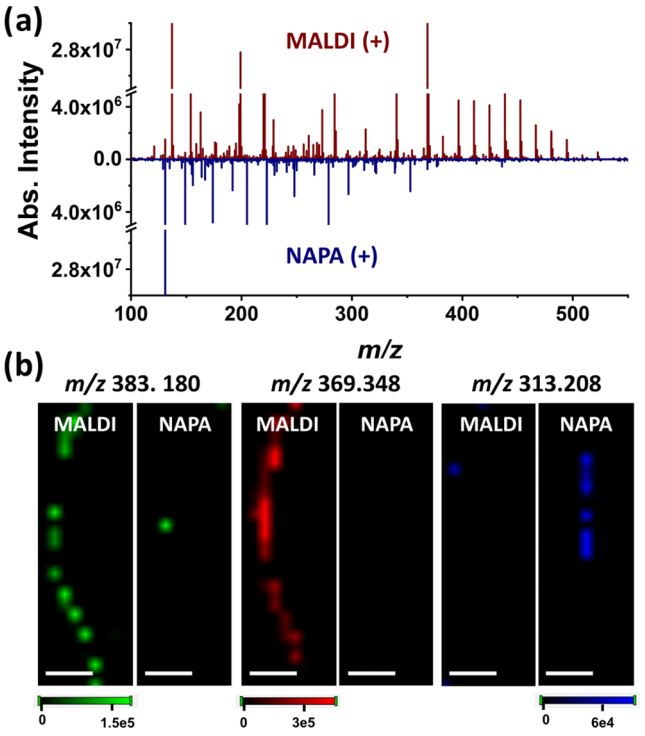

Figure 4. (a) Comparison of MALDI and NAPA−LDI mass spectra from hair section samples. (b) Comparison of MS images for longitudinal scalp hair sections acquired by MALDI−MSI and NAPA−LDI−MSI for spectral features m/z 383.180, m/z 369.348, and m/z 313.208. Scale bars are 500 μm.

CONCLUSIONS

Local analysis from small sampling spots is a prerequisite for the 2D chemical imaging of metabolites and xenobiotics in hard tissues. Two novel ionization methods, LAESI and NAPA−LDI have been tested for local MS analysis and MSI of tooth and hair samples. Local detection of organic molecules, including nicotine metabolites, in the dentin of tooth sections has been demonstrated by LAESI−MS from spot sizes of ∼150 μm. For higher spatial resolution, tighter focusing of the mid-IR laser beam can be achieved by utilizing a reflective objective for focusing or delivering the laser pulse through a sharpened optical fiber.

Local analysis of single hair strands without extensive sample preparation was also explored by LAESI−IMS−MS. Feature-rich spectra (a total of 114 sample-related peaks for male smoker and female nonsmoker sample types) were captured by delivering multiple laser pulses at an elevated fluence. The spatial mapping of organic molecules offered by laser ablation sampling promises insight into the time dependence of past exposures to chemicals or other environmental factors. This is important because other analytical techniques, used as the gold standard for determining the average concentrations of biomarkers in hard tissues (i.e., GC−MS and LC−MS), lack the ability to spatially map biomarker concentrations linked to the temporal dynamics of the exposure.

Incorporation of IMS into LAESI−MS for the rapid separation of ions and the determination of CCS values enhanced the signal-to-noise ratios, reduced the spectral complexity, improved the molecular coverage, and facilitated peak assignments. Using LAESI−IMS−MS, cotinine was detected exclusively in smoker hair and endogenous steroid

https://doi.org/10.1021/acs.analchem.4c00224
Anal. Chem. 2024, 96, 7022−7029

hormones and several lipid species were tentatively identified in all hair samples.

In longitudinally sectioned hair samples, MALDI−MS and NAPA−LDI−MS were applied for the profiling and imaging of chemical species. The two techniques provided highly complementary information, with over 180 sample-related spectral features in the combined spectra. Imaging by these two techniques has been demonstrated with a 100 μm spatial resolution. More confident peak assignments for the collected spectra will require tandem MS measurements.

To ensure well-defined longitudinal sectioning of hair strands, in future studies a new cutting device will be used with a microtome blade mounted at a shallow angle. A cutting block will hold the hair strands in straight grooves at a predefined depth. Moving the cutting device along the grooves shaves off the part of the hair strand protruding above the block surface and exposes the hair interior at predefined depths.[47]

Alternatively, multimodal imaging can be implemented on a single hair section by combining imaging with a lower laser fluence for MALDI−MSI followed by a higher fluence pass for NAPA−LDI−MSI.[46] This approach has been shown to result in imaging with enhanced molecular coverage from the same hair strand. Combining data from LAESI−IMS−MS and NAPA−LDI−MS yields enhanced molecular coverage with quantitation capabilities and spatial resolution that can reveal the distributions of known and potential biomarkers in hard tissues, facilitating exposome research.

The feature-rich spectra generated by untargeted analysis can also be explored by pattern recognition using machine-learning algorithms and correlating them with disease states.[48,49] The comparison of the spectral fingerprints of diseased and control samples might allow for the detection of dysregulated metabolic pathways and unique chemical signatures associated with a particular disease. The characterization of predictive biomarkers at different time points in disease progression and the incorporation of temporal patterns in the training of machine-learning algorithms will facilitate early disease detection and classification of disease states.

■ ASSOCIATED CONTENT

Supporting Information

The Supporting Information is available free of charge at https://pubs.acs.org/doi/10.1021/acs.analchem.4c00224.

Four supporting figures (PDF)

■ AUTHOR INFORMATION

Corresponding Author

Akos Vertes − *Department of Chemistry, The George Washington University, Washington, District of Columbia 20052, United States;* orcid.org/0000-0001-5186-5352; Email: vertes@gwu.edu

Authors

Marjan Dolatmoradi − *Department of Chemistry, The George Washington University, Washington, District of Columbia 20052, United States*

Joanna Ellis − *Department of Environmental Medicine and Public Health, Icahn School of Medicine at Mount Sinai, New York, New York 10029, United States; Linus Biotechnology, North Brunswick, New Jersey 08902, United States*

Christine Austin − *Department of Environmental Medicine and Public Health, Icahn School of Medicine at Mount Sinai, New York, New York 10029, United States*

Manish Arora − *Department of Environmental Medicine and Public Health, Icahn School of Medicine at Mount Sinai, New York, New York 10029, United States; Linus Biotechnology, North Brunswick, New Jersey 08902, United States*

Complete contact information is available at: https://pubs.acs.org/10.1021/acs.analchem.4c00224

Notes

The authors declare no competing financial interest.

■ ACKNOWLEDGMENTS

The research reported in this publication was in part supported by the University Facilitating Funds of The George Washington University (to A.V.), and by awards R35ES030435 and R01ES026033 from the National Institute of Environmental Health Sciences (to M.A.). One of the authors (M.D.) was also supported as a graduate assistant by the Columbian College of Arts and Sciences of The George Washington University.

■ REFERENCES

(1) Jacob, P.; Seidel, A. *J. Chromatogr. B* **2002**, *778*, 31−47, DOI: 10.1016/s0378-4347(01)00467-4.

(2) Humphrey, L. T.; Dean, M. C.; Jeffries, T. E.; Penn, M. *Proc. Natl. Acad. Sci. U.S.A.* **2008**, *105*, 6834−6839.

(3) Bartkus, L.; Amarasiriwardena, D.; Arriaza, B.; Bellis, D.; Yanez, J. *Microchem. J.* **2011**, *98*, 267−274.

(4) Limbeck, A.; Galler, P.; Bonta, M.; Bauer, G.; Nischkauer, W.; Vanhaecke, F. *Anal. Bioanal. Chem.* **2015**, *407*, 6593−6617.

(5) Rodushkin, I.; Axelsson, M. D. *Sci. Total Environ.* **2003**, *305*, 23−39.

(6) Arora, M.; Austin, C. *Curr. Opin. Pediatr.* **2013**, *25*, 261−267.

(7) Stewart, N. A.; Gerlach, R. F.; Gowland, R. L.; Gron, K. J.; Montgomery, J. *Proc. Natl. Acad. Sci. U.S.A.* **2017**, *114*, 13649−13654.

(8) Montag, A. C.; Chambers, C. D.; Jones, K. L.; Dassanayake, P. S.; Andra, S. S.; Petrick, L. M.; Arora, M.; Austin, C.; Collaborative Initiative on Fetal Alcohol Spectrum Disorders (CIFASD). *Birth Defects Res.* **2022**, *114*, 797−804, DOI: 10.1002/bdr2.2054.

(9) Lee, Y.; Seo, E.; Park, J. Y.; Bae, K. H.; Lee, J.; Cha, S. *Mass Spectrom. Lett.* **2018**, *9*, 110−114.

(10) Jagr, M.; Eckhardt, A.; Pataridis, S.; Miksik, I. *Eur. J. Oral Sci.* **2012**, *120*, 259−268.

(11) Andra, S. S.; Austin, C.; Arora, M. *Environ. Res.* **2015**, *142*, 387−406.

(12) Andra, S. S.; Austin, C.; Arora, M. *Curr. Opin. Pediatr.* **2016**, *28*, 221−227.

(13) Yu, M.; Tu, P. J.; Dolios, G.; Dassanayake, P. S.; Volk, H.; Newschaffer, C.; Fallin, M. D.; Croen, L.; Lyall, K.; Schmidt, R.; Hertz-Piccioto, I.; Austin, C.; Arora, M.; Petrick, L. M. *Environ. Int.* **2021**, *157*, No. 106849.

(14) Andra, S. S.; Austin, C.; Wright, R. O.; Arora, M. *Environ. Int.* **2015**, *83*, 137−145.

(15) Cornett, D. S.; Reyzer, M. L.; Chaurand, P.; Caprioli, R. M. *Nat. Methods* **2007**, *4*, 828−833.

(16) Nemes, P.; Vertes, A. *Anal. Chem.* **2007**, *79*, 8098−8106.

(17) Nemes, P.; Barton, A. A.; Vertes, A. *Anal. Chem.* **2009**, *81*, 6668−6675.

(18) Li, H.; Smith, B. K.; Mark, L.; Nemes, P.; Nazarian, J.; Vertes, A. *Int. J. Mass Spectrom.* **2015**, *377*, 681−689.

(19) Stopka, S. A.; Wood, E. A.; Khattar, R.; Agtuca, B. J.; Abdelmoula, W. M.; Agar, N. Y. R.; Stacey, G.; Vertes, A. *Anal. Chem.* **2021**, *93*, 9677−9687.

(20) Walker, B. N.; Stolee, J. A.; Pickel, D. L.; Retterer, S. T.; Vertes, A. *J. Phys. Chem. C* **2010**, *114*, 4835−4840.
(21) Walker, B. N.; Stolee, J. A.; Vertes, A. *Anal. Chem.* **2012**, *84*, 7756−7762.
(22) Stopka, S. A.; Rong, C.; Korte, A. R.; Yadavilli, S.; Nazarian, J.; Razunguzwa, T. T.; Morris, N. J.; Vertes, A. *Angew. Chem., Int. Ed.* **2016**, *55*, 4482−4486.
(23) Korte, A. R.; Morris, N. J.; Vertes, A. *Anal. Chem.* **2019**, *91*, 3951−3958.
(24) Buckley, M.; Kansa, S. W. *Archaeol. Anthropol. Sci.* **2011**, *3*, 271−280, DOI: 10.1007/s12520-011-0066-z.
(25) Good, C. J.; Neumann, E. K.; Butrico, C. E.; Cassat, J. E.; Caprioli, R. M.; Spraggins, J. M. *Anal. Chem.* **2022**, *94*, 3165−3172.
(26) Poetzsch, M.; Steuer, A. E.; Roemmelt, A. T.; Baumgartner, M. R.; Kraemer, T. *Anal. Chem.* **2014**, *86*, 11758−11765.
(27) Porta, T.; Grivet, C.; Kraemer, T.; Varesio, E.; Hopfgartner, G. *Anal. Chem.* **2011**, *83*, 4266−4272.
(28) Henderson, G. L. *Forensic Sci. Int.* **1993**, *63*, 19−29.
(29) Nemes, P.; Woods, A. S.; Vertes, A. *Anal. Chem.* **2010**, *82*, 982−988.
(30) Nemes, P.; Vertes, A. *TrAC, Trends Anal. Chem.* **2012**, *34*, 22−34, DOI: 10.1016/j.trac.2011.11.006.
(31) Shrestha, B.; Vertes, A. *Anal. Chem.* **2014**, *86*, 4308−4315.
(32) Duca, R. C.; Hardy, E.; Salquebre, G.; Appenzeller, B. M. R. *Drug Test. Anal.* **2014**, *6*, 55−66, DOI: 10.1002/dta.1649.
(33) Morris, N. J.; Anderson, H.; Thibeault, B.; Vertes, A.; Powell, M. J.; Razunguzwa, T. T. *RSC Adv.* **2015**, *5*, 72051−72057.
(34) Xu, C. Q.; Yao, X. M.; Walker, M. P.; Wang, Y. *Calcif. Tissue Int.* **2009**, *84*, 221−228, DOI: 10.1007/s00223-008-9212-8.
(35) Kim, I.; Darwin, W. D.; Huestis, M. A. *J. Chromatogr. B* **2005**, *814*, 233−240.
(36) Shiraishi, S.; Lee, P. W. N.; Leung, A.; Goh, V. H. H.; Swerdloff, R. S.; Wang, C. *Clin. Chem.* **2008**, *54*, 1855−1863.
(37) Kjeld, J. M.; Puah, C. M.; Joplin, G. F. *Br. Med. J.* **1976**, *2*, 1354−1356.
(38) Grymowicz, M.; Rudnicka, E.; Podfigurna, A.; Napierala, P.; Smolarczyk, R.; Smolarczyk, K.; Meczekalski, B. *Int. J. Mol. Sci.* **2020**, *21*, 5342.
(39) Chouinard, C. D.; Beekman, C. R.; Kemperman, R. H. J.; King, H. M.; Yost, R. A. *Int. J. Ion Mobility Spectrom.* **2017**, *20*, 31−39, DOI: 10.1007/s12127-016-0213-4.
(40) Gao, W.; Kirschbaum, C.; Grass, J.; Stalder, T. *J. Steroid Biochem. Mol. Biol.* **2016**, *162*, 92−99, DOI: 10.1016/j.jsbmb.2015.12.022.
(41) Scherer, C.; Wachter, U.; Wudy, S. A. *Analyst* **1998**, *123*, 2661−2663.
(42) Morley, J. E.; Patrick, P.; Perry, H. M. *Metab., Clin. Exp.* **2002**, *51*, 554−559, DOI: 10.1053/meta.2002.31975.
(43) Schallreuter, K. U.; Beazley, W. D.; Hibberts, N. A.; Tobin, D. J.; Paus, R.; Wood, J. M. *J. Invest. Dermatol.* **1998**, *111*, 545−550.
(44) Lee, W. S. *J. Dermatol. Sci.* **2011**, *64*, 153−158.
(45) Boumba, V. A.; Ziavrou, K. S.; Vougiouklakis, T. *Int. J. Toxicol.* **2006**, *25*, 143−163.
(46) Fincher, J. A.; Korte, A. R.; Yadavilli, S.; Morris, N. J.; Vertes, A. *Analyst* **2020**, *145*, 6910−6918.
(47) Flinders, B.; Cuypers, E.; Zeijlemaker, H.; Tytgat, J.; Heeren, R. M. A. *Drug Test. Anal.* **2015**, *7*, 859−865, DOI: 10.1002/dta.1812.
(48) Curtin, P.; Austin, C.; Curtin, A.; Gennings, C.; Arora, M.; Tammimies, K.; Willfors, C.; Berggren, S.; Siper, P.; Rai, D.; Meyering, K.; Kolevzon, A.; Mollon, J.; David, A. S.; Lewis, G.; Zammit, S.; Heilbrun, L.; Palmer, R. F.; Wright, R. O.; Bolte, S.; Reichenberg, A. *Sci. Adv.* **2018**, *4*, No. eaat1293, DOI: 10.1126/sciadv.aat1293.
(49) Austin, C.; Curtin, P.; Arora, M.; Reichenberg, A.; Curtin, A.; Iwai-Shimada, M.; Wright, R. O.; Wright, R. J.; Remnelius, K. L.; Isaksson, J.; Bolte, S.; Nakayama, S. F. *J. Clin. Med.* **2022**, *11*, 7154.

https://doi.org/10.1021/acs.analchem.4c00224
Anal. Chem. 2024, 96, 7022−7029

Supporting Information

Detection and Imaging of Exposure-Related Metabolites and Xenobiotics in Hard Tissues by Laser Sampling and Mass Spectrometry

Marjan Dolatmoradi,[a] Joanna Ellis,[b,c] Christine Austin,[b] Manish Arora,[b,c] and Akos Vertes[a,]*

[a]*Department of Chemistry, The George Washington University, Washington, District of Columbia 20052, United States*

[b]*Department of Environmental Medicine and Public Health, Icahn School of Medicine at Mount Sinai, New York, New York 10029, United States*

[c]*Linus Biotechnology, North Brunswick, New Jersey 08902, United States*

*Corresponding author
E-mail: vertes@gwu.edu

Table of Contents

Figure S1. Two novel laser based soft ionization methods for hard tissue analysis……..3

Figure S2. Significantly regulated spectral features for smoker and non-smoker hair samples…4

Figure S3. Tandem MS for *m/z* 220.087 ion from hair sample……..……5

Figure S4. Longitudinal sections of single scalp hair for MALDI-MSI and NAPA-LDI-MSI.....6

Figures

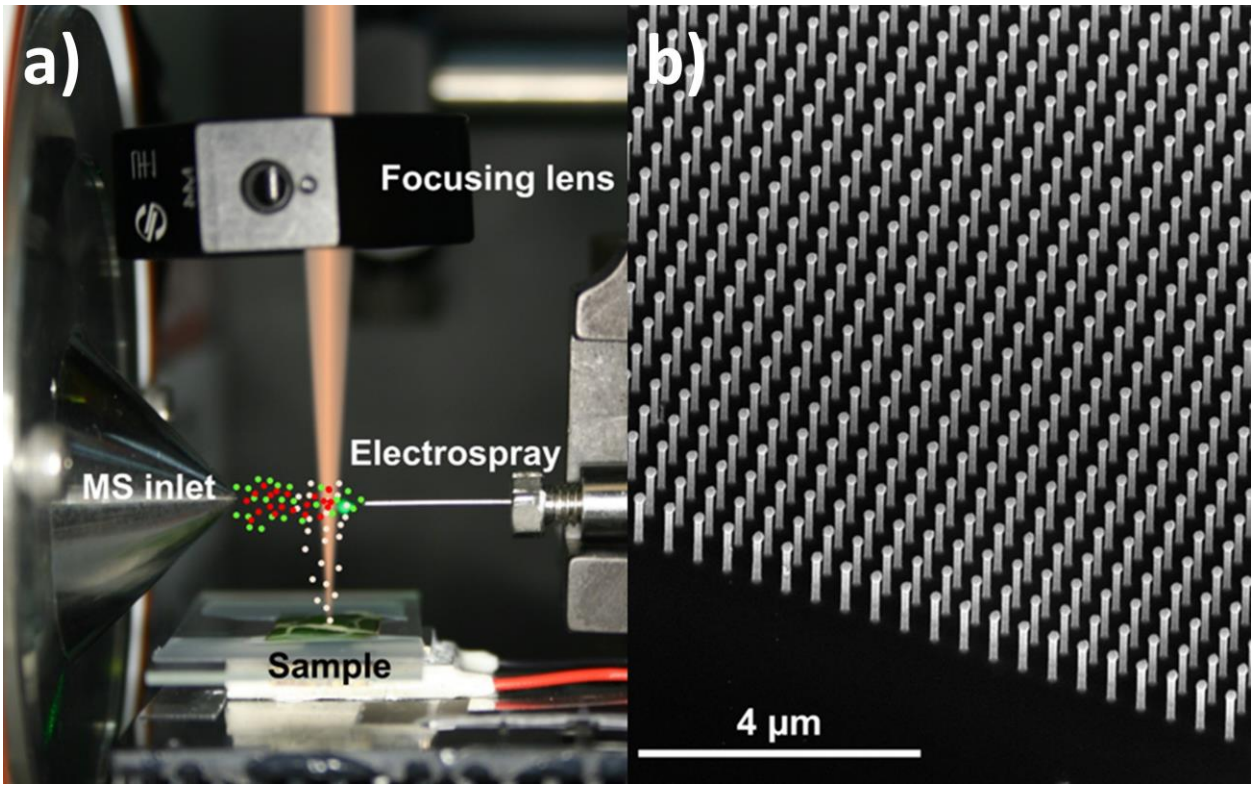

Figure S1. Two laser based soft ionization methods utilized for hard tissue analysis. **(a)** A LAESI ion source coupled to a mass spectrometer inlet. Beige, green, and red dots represent laser ablated particles, electrospray droplets, and droplets formed by their coalescence, respectively. **(b)** Silicon nanopost array substrate designed for NAPA-LDI-MS imaging.

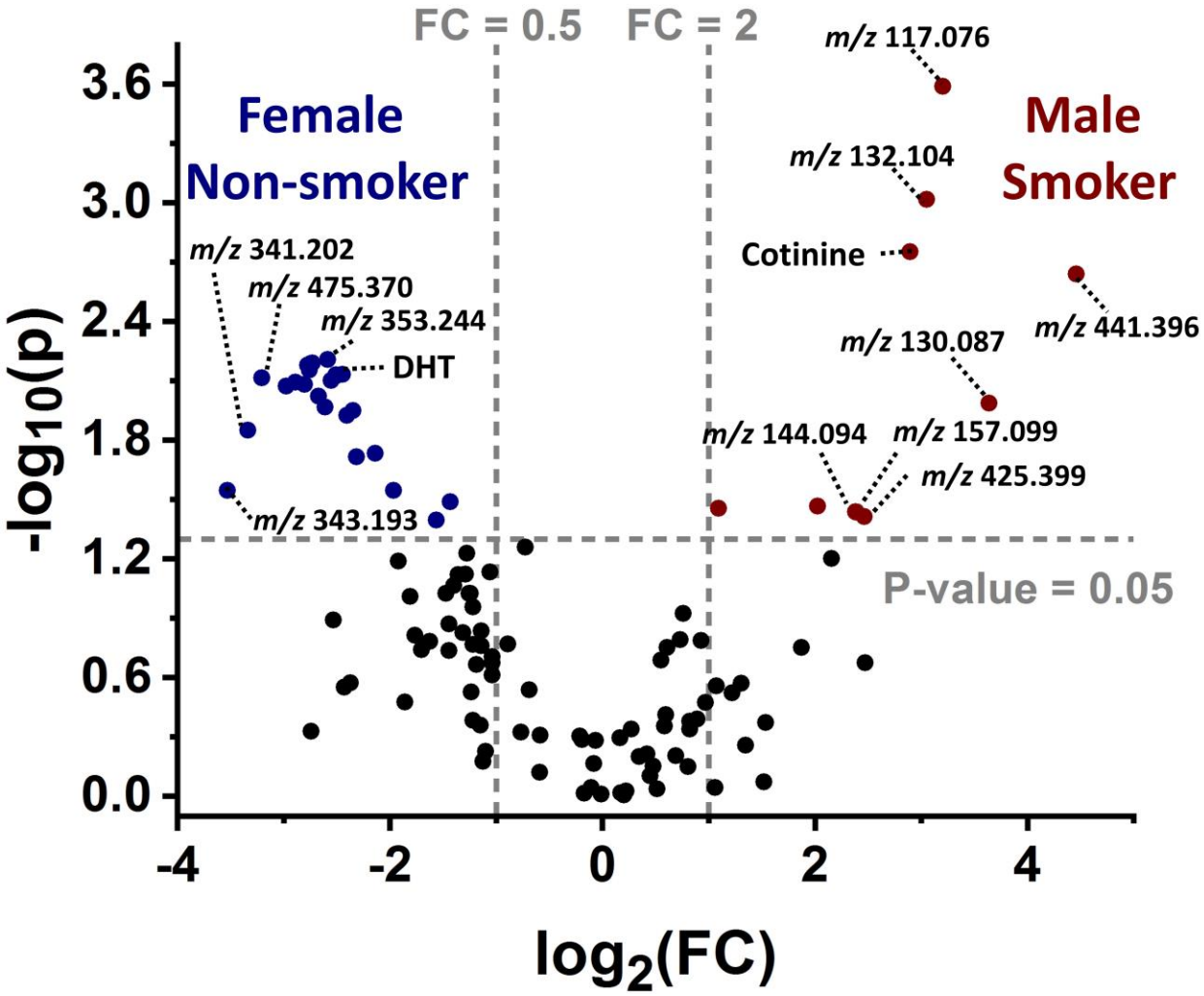

Figure S2. Volcano plot for significantly up- and down-regulated spectral features detected in smoker and non-smoker hair samples. For cotinine, the assignment is based on $\Delta m/z$ = 0.2 mDa between the measured and calculated *m/z* values for $[M+H]^+$, the tandem MS in Figure 2b, and CCS data (ΔCCS = -4.4 Å^2). For protonated DHT the figures are $\Delta m/z$ = -6.0 mDa and ΔCCS = -4.8 Å^2, and there is no tandem MS data.

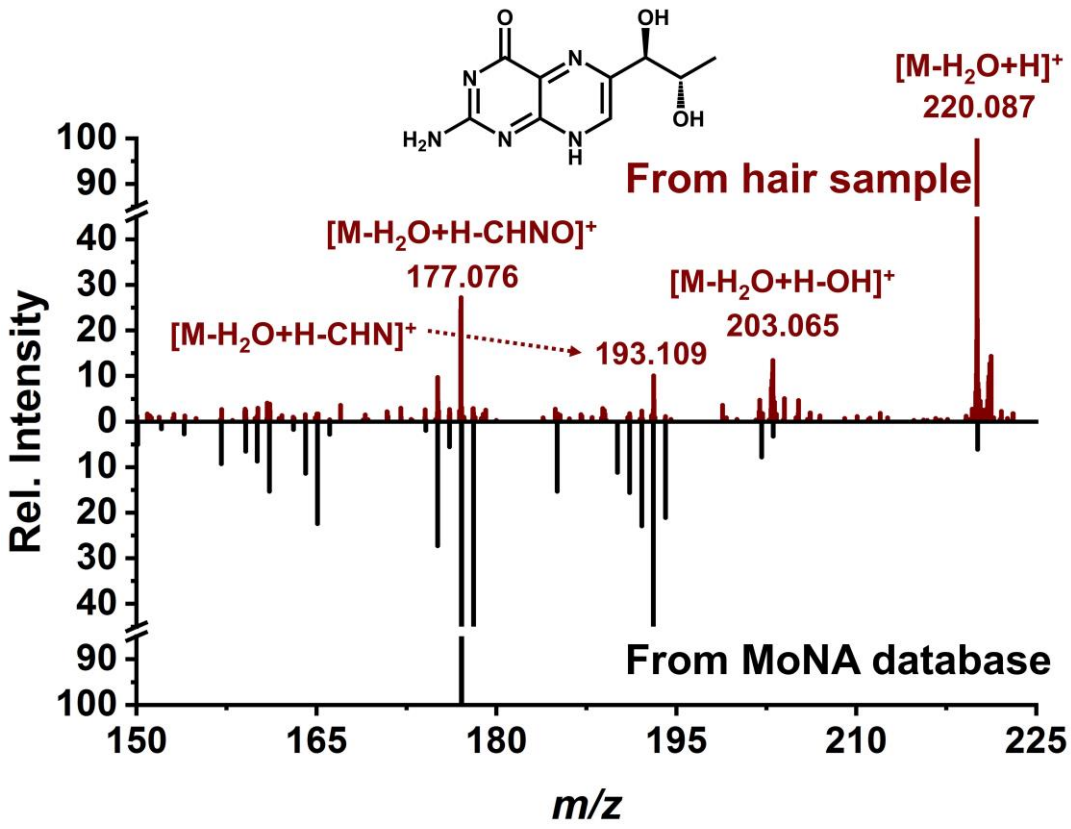

Figure S3. Tandem MS of *m/z* 220.087 ion from hair sample (top spectrum) shows similar fragmentation to biopterin entry (bottom spectrum) in MoNA database (https://mona.fiehnlab.ucdavis.edu/). The difference between the measured and calculated *m/z* values for the fragments are as follows: Δ*m/z* = 4 mDa for $[M\text{-}H_2O+H]^+$, Δ*m/z* = -16 mDa for $[M\text{-}H_2O\text{+}H\text{-}OH]^+$, Δ*m/z* = 36 mDa for $[M\text{-}H_2O\text{+}H\text{-}CHN]^+$, and Δ*m/z* = -2 mDa for $[M\text{-}H_2O\text{+}H\text{-}CHNO]^+$.

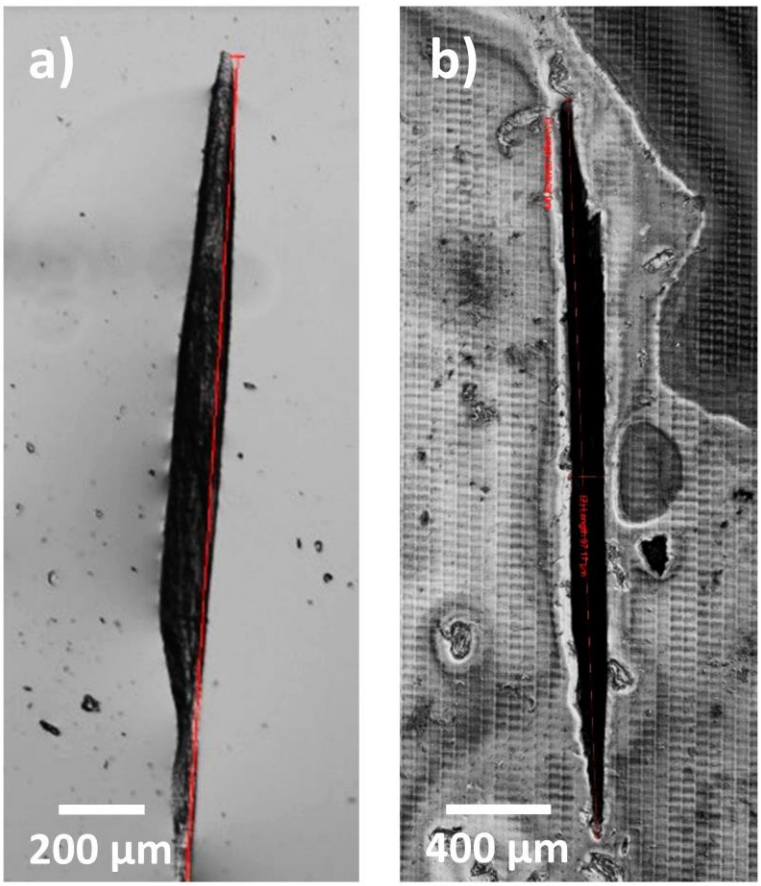

Figure S4. Splitting hair. Longitudinal sections of single scalp hair strands thaw-mounted onto (a) a microscope slide for MALDI-MSI, and (b) a NAPA nanostructure for LDI-MSI.